 CMC, vol.15, no.1, pp.1-25, 2010

Meshless Local Petrov-Galerkin (MLPG) Method for Laminate Plates under Dynamic Loading

J. Sladek[1], **V. Sladek**[1], **P. Stanak**[1] **and Ch. Zhang**[2]

Abstract: A meshless local Petrov-Galerkin (MLPG) method is applied to solve laminate plate problems described by the Reissner-Mindlin theory. Both stationary and transient dynamic loads are analyzed here. The bending moment and the shear force expressions are obtained by integration through the laminated plate for the considered constitutive equations in each lamina. The Reissner-Mindlin theory reduces the original three-dimensional (3-D) thick plate problem to a two-dimensional (2-D) problem. Nodal points are randomly distributed over the mean surface of the considered plate. Each node is the center of a circle surrounding this node. The weak-form on small subdomains with a Heaviside step function as the test functions is applied to derive local integral equations. After performing the spatial MLS approximation, a system of ordinary differential equations of the second order for certain nodal unknowns is obtained. The derived ordinary differential equations are solved by the Houbolt finite-difference scheme as a time-stepping method.

Keywords: Local integral equations, Reissner-Mindlin plate theory, Houbolt finite-difference scheme, MLS approximation, orthotropic material properties

1 Introduction

Laminated composite plates are widely applied in engineering structures because they can be optimized to satisfy the high-performance requirements according to different in-service conditions. Much previous research works have been done for static and dynamic analysis of isotropic thin plates. Previous research results show that the transverse shear effects are more significant for orthotropic plates than for isotropic ones [Wang and Huang (1991), Wang and Schweizerhof (1996)]. It is well known that the classical thin plate theory of Kirchhoff gives rise to certain non-

[1] Institute of Construction and Architecture, Slovak Academy of Sciences, 84503 Bratislava, Slovakia
[2] Department of Civil Engineering, University of Siegen, D-57068 Siegen, Germany

physical simplifications mainly related to the omission of the shear deformation and the rotary inertia, which become more significant for increasing thickness of the plate. The effects of shear deformation and rotary inertia are taken into account in the Reissner (1946), Mindlin (1951) plate bending theory and higher order shear theories [Reddy, 1997]. They are widely accepted and applied to many engineering problems. Suetake (2006) modified the high-order bending theory of plates by constitution of the lateral loads through consideration of the transverse normal stress. The effects of shear deformation and rotary inertia following Reissner-Mindlin's plate theory are included in the elastoplastic transient response of plates with all possible boundary conditions on edges and any interior support conditions such as isolated points (columns), lines (walls) or regions (patches) by Providakis (2007). Wen and Hon (2007) used smooth radial basis functions for the geometrically nonlinear analysis of Reissner-Mindlin plates. Pagano (1969) obtained analytical solutions for simply supported orthotropic laminates. This benchmark solution has been used to validate new or improved plate theories and finite element formulations [Murakami (1986); Mau, Tong and Pian (1972)]. Three-dimensional deformations of multilayered, linear elastic, anisotropic rectangular plates are analyzed by Vel and Batra (1999). Later, Vel and Batra (2000) used the Eshelby-Stroh formalism to analyze the cylindrical bending of anisotropic and linear elastic laminate plates. They extended their theory to quasi-static thermoelastic deformations of laminated anisotropic thick plates [Vel and Batra (2001)]. Smojver and Soric (2007) have applied FEM (ABAQUS) to consider delamination for layered composite plates.

The solution of the boundary or initial boundary value problems for laminated anisotropic plates requires advanced numerical methods due to the high mathematical complexity. Beside the well established finite element method (FEM), the boundary element method (BEM) provides an efficient and popular alternative to the FEM. The conventional BEM is accurate and efficient for many engineering problems. However, it requires the availability of the fundamental solutions or Green's functions to the governing partial differential equations (PDE). The material anisotropy increases the number of elastic constants in Hooke's law, and hence makes the construction of the fundamental solutions cumbersome. The elimination of shear locking in thin walled structures by FEM is difficult and the developed techniques are less accurate. Meshless methods for solving PDE in physics and engineering sciences are a powerful new alternative to the traditional mesh-based techniques. Focusing only on nodes or points instead of elements used in the conventional FEM or BEM, meshless approaches have certain advantages. The moving least-square (MLS) approximation ensures C^1 continuity which satisfies the Kirchhoff hypotheses. The continuity of the MLS approximation is given by the minimum between the continuity of the basis functions and that of the weight function.

So continuity can be tuned to a desired degree. The results showed excellent convergence, however, the formulation is not applicable to shear deformable laminated plate problems up to date. One of the most rapidly developed meshfree methods is the meshless local Petrov-Galerkin (MLPG) method. The MLPG method has attracted much attention during the past decade [Atluri and Zhu, 1998; Atluri at al. 2000; Atluri, 2004; Han et al., 2003; Mikhailov, 2002; Sellountos et al., 2005; Liu et al., 2006; Vavourakis and Polyzos, 2007] for many problems of continuum mechanics. Recent successes of the MLPG methods have been reported in solving a 4^{th} order ordinary differential equation [Atluri and Shen (2005)]; in the development of a nonlinear formulation of the MLPG finite-volume mixed method for the large deformation analysis of static and dynamic problems [Han et al (2005)]; in simplified treatment of essential boundary conditions by a novel modified MLS procedure [Gao et al (2006)]; in analysis of transient thermomechanical response of functionally graded composites [Ching and Chen (2006)]; in the ability for solving high-speed contact, impact and penetration problems with large deformations and rotations [Han et al (2006)]; in the development of the mixed scheme to interpolate the elastic displacements and stresses independently [Atluri et al (2006a), (2006b)]; in proposal of a direct solution method for the quasi-unsymmetric sparse matrix arising in the MLPG [Yuan et al (2007)]; and in the development of the MLPG using the Dirac delta function as the test function for 2D heat conduction problems in irregular domain [Wu et al (2007)].

In the present paper we will present for the first time a meshless method based on the local Petrov-Galerkin weak-form to solve dynamic problems for laminated plate bending described by the Reissner-Mindlin theory. The bending moment and the shear force expressions are obtained by integration through the laminated plate for the considered constitutive equations in each lamina. The Reissner-Mindlin governing equations of motion are subsequently solved for an elastodynamic plate bending problem. The Reissner-Mindlin theory reduces the original three-dimensional (3-D) thick plate problem to a two-dimensional (2-D) problem. In our meshless method, nodal points are randomly distributed over the mean surface of the considered plate. Each node is the center of a circle surrounding this node. A similar approach has been successfully applied to a thin Kirchhoff plate [Sladek et al., 2002, 2003] where the governing equation is decomposed into two partial differential equations (PDE) of the second order [De Leon and Paris, 1987]. Long and Atluri (2002) applied the meshless local Petrov Galerkin method to solve the bending problem of a thin plate. The MLPG method has been also applied to Reissner-Mindlin plates and shells under dynamic load by Sladek et al. (2007, 2006). Soric et al. (2004) have performed a three-dimensional analysis of thick plates, where a plate is divided by small cylindrical subdomains for which the MLPG is applied.

Homogeneous material properties of plates are considered in previous papers. Recently, Qian et al. (2004) extended the MLPG for 3-D deformations in thermoelastic bending of functionally graded isotropic plates.

The weak-form on small subdomains with a Heaviside step function as the test functions is applied to derive local integral equations. Applying the Gauss divergence theorem to the weak-form, the local boundary-domain integral equations are derived. After performing the spatial MLS approximation, a system of ordinary differential equations for certain nodal unknowns is obtained. Then, the system of the ordinary differential equations of the second order resulting from the equations of motion is solved by the Houbolt finite-difference scheme [Houbolt (1950)] as a time-stepping method. Numerical examples are presented and discussed to show the accuracy and the efficiency of the present method.

2 Local integral equations for laminated plate theory

The classical laminate plate theory is an extension of the classical plate theory to composite laminates. Consider a plate of total thickness h composed of N orthotropic layers with the mean surface occupying the domain Ω in the plane (x_1, x_2). The $x_3 \equiv z$ axis is perpendicular to the mid-plane (Fig.1). The k-th layer is located between the points $z = z_k$ and $z = z_{k+1}$ in the thickness direction.

The Reissner-Mindlin plate bending theory [Reissner, 1946; Mindlin, 1951] is used to describe the plate deformation. The transverse shear strains are represented as constant throughout the plate thickness and some correction coefficients are required for the computation of transverse shear forces in that theory. Then, the spatial displacement field in time τ, due to transverse loading and expressed in terms of displacement components u_1, u_2 and u_3, has the following form [Reddy, 1997]

$$
\begin{aligned}
&u_1(\mathbf{x}, x_3, \tau) = x_3 w_1(\mathbf{x}, \tau), \\
&u_2(\mathbf{x}, x_3, \tau) = x_3 w_2(\mathbf{x}, \tau), \\
&u_3(\mathbf{x}, \tau) = w_3(\mathbf{x}, \tau),
\end{aligned}
\tag{1}
$$

where $\mathbf{x} = [x_1, x_2]^T$ is the position vector, $w_\alpha(x_1, x_2, \tau)$ and $w_3(x_1, x_2, \tau)$ represent the rotations around the in-plane axes and the out-of-plane deflection, respectively (Fig. 1).

The linear strains are given by

$$
\varepsilon_{11}(\mathbf{x}, x_3, \tau) = x_3 w_{1,1}(\mathbf{x}, \tau),
$$

$$
\varepsilon_{22}(\mathbf{x}, x_3, \tau) = x_3 w_{2,2}(\mathbf{x}, \tau),
$$

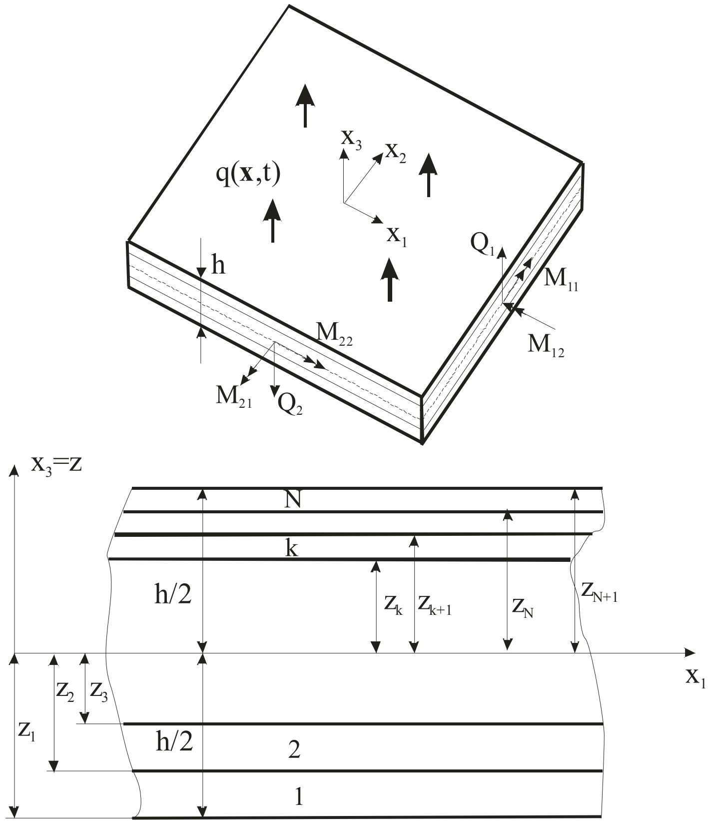

Figure 1: Sign convention of bending moments, forces and layer numbering for a laminate plate

$$\varepsilon_{12}(\mathbf{x},x_3,\tau) = x_3\left[w_{1,2}(\mathbf{x},\tau)+w_{2,1}(\mathbf{x},\tau)\right]/2,$$
$$\varepsilon_{13}(\mathbf{x},\tau) = \left[w_1(\mathbf{x},\tau)+w_{3,1}(\mathbf{x},\tau)\right]/2,$$
$$\varepsilon_{23}(\mathbf{x},\tau) = \left[w_2(\mathbf{x},\tau)+w_{3,2}(\mathbf{x},\tau)\right]/2. \tag{2}$$

In the case of orthotropic materials for the k-th lamina, the relation between the stresses σ_{ij} and the strains ε_{ij} is described by the constitutive equations for the stress tensor

$$\sigma_{ij}^{(k)}(\mathbf{x},x_3,\tau) = c_{ijml}^{(k)}\varepsilon_{ml}(\mathbf{x},x_3,\tau), \tag{3}$$

where the material stiffness coefficients $c_{ijml}^{(k)}$ are assumed to be homogeneous for the k-th lamina.

It can be seen from equation (2) that the strains are continuous throughout the plate thickness. Hence, discontinuous material coefficients yield discontinuities in stresses on the lamina surfaces.

For plane problems the constitutive equation (3) is frequently written in terms of the second-order tensor of elastic constants [Lekhnitskii (1963)]. The constitutive equation for orthotropic materials and plane stress problem has the following form

$$\begin{bmatrix}\sigma_{11}\\ \sigma_{22}\\ \sigma_{12}\\ \sigma_{13}\\ \sigma_{23}\end{bmatrix}^{(k)} = \mathbf{G}^{(k)}(\mathbf{x}) \begin{bmatrix}\varepsilon_{11}\\ \varepsilon_{22}\\ 2\varepsilon_{12}\\ 2\varepsilon_{13}\\ 2\varepsilon_{23}\end{bmatrix}, \tag{4}$$

where

$$\mathbf{G}^{(k)}(\mathbf{x}) = \begin{bmatrix} E_1^{(k)}/e^{(k)} & E_1^{(k)}\nu_{21}^{(k)}/e^{(k)} & 0 & 0 & 0\\ E_2^{(k)}\nu_{12}^{(k)}/e^{(k)} & E_2^{(k)}/e^{(k)} & 0 & 0 & 0\\ 0 & 0 & G_{12}^{(k)} & 0 & 0\\ 0 & 0 & 0 & G_{13}^{(k)} & 0\\ 0 & 0 & 0 & 0 & G_{23}^{(k)} \end{bmatrix}$$

with $e^{(k)} = 1-\nu_{12}^{(k)}\nu_{21}^{(k)}$, $E_\alpha^{(k)}$ are the Young's moduli refering to the axes $x_\alpha (\alpha = 1, 2)$, $G_{12}^{(k)}$, $G_{13}^{(k)}$ and $G_{23}^{(k)}$ are shear moduli, and $\nu_{\alpha\beta}$ are Poisson's ratios.

Despite the stress discontinuities, one can define the integral quantities such as the bending moments $M_{\alpha\beta}$ and the shear forces Q_α as

$$\begin{bmatrix}M_{11}\\ M_{22}\\ M_{12}\end{bmatrix} = \int_{-h/2}^{h/2} \begin{bmatrix}\sigma_{11}\\ \sigma_{22}\\ \sigma_{12}\end{bmatrix} x_3 dx_3 = \sum_{k=1}^{N} \int_{z_k}^{z_{k+1}} \begin{bmatrix}\sigma_{11}\\ \sigma_{22}\\ \sigma_{12}\end{bmatrix}^{(k)} x_3 dx_3$$

and

$$\begin{bmatrix}Q_1\\ Q_2\end{bmatrix} = \kappa \int_{-h/2}^{h/2} \begin{bmatrix}\sigma_{13}\\ \sigma_{23}\end{bmatrix} dx_3 = \kappa \sum_{k=1}^{N} \int_{z_k}^{z_{k+1}} \begin{bmatrix}\sigma_{13}\\ \sigma_{23}\end{bmatrix}^{(k)} dx_3, \tag{5}$$

where $\kappa = 5/6$ in the Reissner plate theory.

Substituting equations (4) and (2) into moment and force resultants (5) allows the expression of the bending moments $M_{\alpha\beta}$ and shear forces Q_α for α, β=1,2, in terms of rotations and lateral displacements of the orthotropic plate. In the case of the considered layer-wise continuous material properties through the plate thickness, one obtains

$$M_{\alpha\beta} = D_{\alpha\beta}\left(w_{\alpha,\beta} + w_{\beta,\alpha}\right) + C_{\alpha\beta} w_{\gamma,\gamma},$$

$$Q_{\alpha} = C_{\alpha}\left(w_{\alpha} + w_{3,\alpha}\right). \tag{6}$$

In eq. (6), repeated indices α and β do not imply summation, and the material parameters $D_{\alpha\beta}$ and $C_{\alpha\beta}$ are given as

$$2D_{11} = \int_{-h/2}^{h/2} z^2 E_1(z) \frac{1-\nu_{21}}{e} dz = \sum_{k=1}^{N} \int_{z_k}^{z_{k+1}} E_1^{(k)} \frac{1-\nu_{21}^{(k)}}{e^{(k)}} z^2 dz = \sum_{k=1}^{N} E_1^{(k)} \frac{1-\nu_{21}^{(k)}}{e^{(k)}} \frac{1}{3}\left(z_{k+1}^3 - z_k^3\right),$$

$$2D_{22} = \int_{-h/2}^{h/2} z^2 E_2(z) \frac{1-\nu_{12}}{e} dz = \sum_{k=1}^{N} E_2^{(k)} \frac{1-\nu_{12}^{(k)}}{e^{(k)}} \frac{1}{3}\left(z_{k+1}^3 - z_k^3\right),$$

$$D_{12} = \int_{-h/2}^{h/2} z^2 G_{12}(z) dz = \sum_{k=1}^{N} G_{12}^{(k)} \frac{1}{3}\left(z_{k+1}^3 - z_k^3\right),$$

$$C_{11} = \int_{-h/2}^{h/2} z^2 E_1(z) \frac{\nu_{21}}{e} dz = \sum_{k=1}^{N} E_1^{(k)} \frac{\nu_{21}^{(k)}}{e^{(k)}} \frac{1}{3}\left(z_{k+1}^3 - z_k^3\right),$$

$$C_{22} = \int_{-h/2}^{h/2} z^2 E_2(z) \frac{\nu_{12}}{e} dz = \sum_{k=1}^{N} E_2^{(k)} \frac{\nu_{12}^{(k)}}{e^{(k)}} \frac{1}{3}\left(z_{k+1}^3 - z_k^3\right),$$

$$C_{12} = C_{21} = 0,$$

$$C_{\alpha} = \kappa \int_{-h/2}^{h/2} G_{\alpha 3}(z) dz = \kappa \sum_{k=1}^{N} G_{\alpha 3}^{(k)} \left(z_{k+1} - z_k\right). \tag{7}$$

For a homogeneous plate equations (7) are reduced into simple forms

$$D_{11} = \frac{D_1}{2}\left(1-\nu_{21}\right), \quad D_{22} = \frac{D_2}{2}\left(1-\nu_{12}\right), \quad D_{12} = D_{21} = \frac{G_{12} h^3}{12},$$

$$C_{11} = D_1 \nu_{21}, \quad C_{22} = D_2 \nu_{12}, \quad C_{12} = C_{21} = 0,$$

$$D_{\alpha} = \frac{E_{\alpha} h^3}{12e}, \quad D_1 \nu_{21} = D_2 \nu_{12}, \quad C_{\alpha} = \kappa h G_{\alpha 3}, \tag{8}$$

The plate is subjected to a transverse dynamic load $q(\mathbf{x}, \tau)$. Assuming the mass density to be homogeneous within each lamina and using the Reissner's linear theory of thick plates [Reissner, 1946], the equations of motion may be written as

$$M_{\alpha\beta,\beta}(\mathbf{x},\tau) - Q_{\alpha}(\mathbf{x},\tau) = I_M \ddot{w}_{\alpha}(\mathbf{x},\tau), \tag{9}$$

$$Q_{\alpha,\alpha}(\mathbf{x},\tau)+q(\mathbf{x},\tau)=I_Q\ddot{w}_3(\mathbf{x},\tau), \quad \mathbf{x}\in\Omega, \tag{10}$$

where

$$I_M=\int_{-h/2}^{h/2} z^2\rho(z)dz=\sum_{k=1}^{N}\int_{z_k}^{z_{k+1}}\rho^{(k)}z^2dz=\sum_{k=1}^{N}\rho^{(k)}\frac{1}{3}\left(z_{k+1}^3-z_k^3\right),$$

$$I_Q=\int_{-h/2}^{h/2}\rho(z)dz=\sum_{k=1}^{N}\int_{z_k}^{z_{k+1}}\rho^{(k)}dz=\sum_{k=1}^{N}\rho^{(k)}\left(z_{k+1}-z_k\right)$$

are global inertial characteristics of the laminate plate. If the mass density is constant throughout the plate thickness, we obtain

$$I_M=\frac{\rho h^3}{12}, \quad I_Q=\rho h.$$

Throughout the analysis, Greek indices vary from 1 to 2, and the dots over a quantity indicate differentiations with respect to time τ.

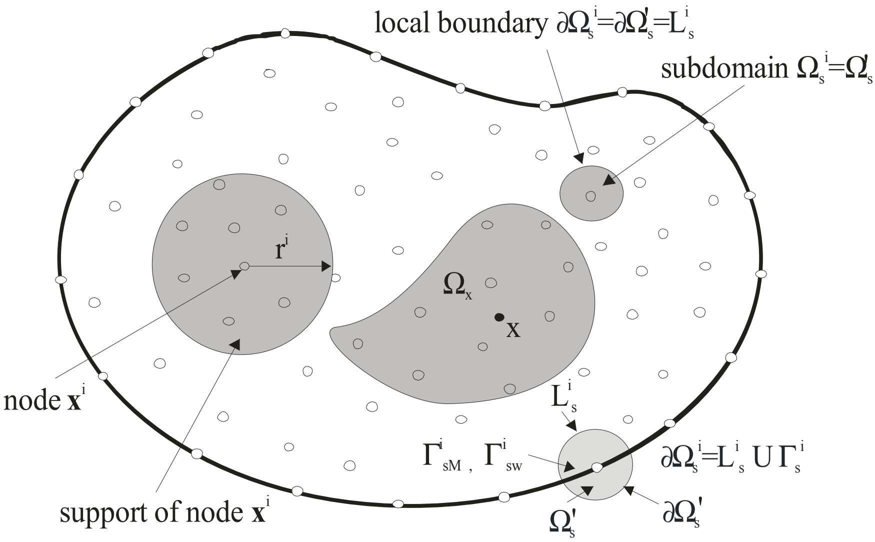

Figure 2: Local boundaries for weak formulation, the domain Ω_x for MLS approximation of the trial function, and support area of weight function around node $\mathbf{x}^i$.

Instead of writing the global weak-form for the above governing equations, the MLPG methods construct the weak-form over local subdomains such as Ω_s, which is a small region taken for each node inside the global domain [Atluri, 2004]. The local subdomains overlap each other and cover the whole global domain Ω (Fig. 2). The local subdomains could be of any geometrical shape and size. In the current paper, the local subdomains are taken to be of circular shape. The local weak-form of the governing equations (9) and (10) for $\mathbf{x}^i \in \Omega_s^i$ can be written as

$$\int\limits_{\Omega_s^i} \left[M_{\alpha\beta,\beta}(\mathbf{x},\tau) - Q_\alpha(\mathbf{x},\tau) - I_M \ddot{w}_\alpha(\mathbf{x},\tau)\right] w^*_{\alpha\gamma}(\mathbf{x}) d\Omega = 0, \tag{11}$$

$$\int\limits_{\Omega_s^i} \left[Q_{\alpha,\alpha}(\mathbf{x},\tau) + q(\mathbf{x},\tau) - I_Q \ddot{w}_3(\mathbf{x},\tau)\right] w^*(\mathbf{x}) d\Omega = 0, \tag{12}$$

where $w^*_{\alpha\beta}(\mathbf{x})$ and $w^*(\mathbf{x})$ are weight or test functions.
Applying the Gauss divergence theorem to Eqs. (11) and (12) one obtains

$$\int\limits_{\partial\Omega_s^i} M_\alpha(\mathbf{x},\tau) w^*_{\alpha\gamma}(\mathbf{x}) d\Gamma - \int\limits_{\Omega_s^i} M_{\alpha\beta}(\mathbf{x},\tau) w^*_{\alpha\gamma,\beta}(\mathbf{x}) d\Omega - \int\limits_{\Omega_s^i} Q_\alpha(\mathbf{x},\tau) w^*_{\alpha\gamma}(\mathbf{x}) d\Omega -$$

$$- \int\limits_{\Omega_s^i} I_M \ddot{w}_\alpha(\mathbf{x},\tau) w^*_{\alpha\gamma}(\mathbf{x}) d\Omega = 0, \tag{13}$$

$$\int\limits_{\partial\Omega_s^i} Q_\alpha(\mathbf{x},\tau) n_\alpha(\mathbf{x}) w^*(\mathbf{x}) d\Gamma - \int\limits_{\Omega_s^i} Q_\alpha(\mathbf{x},\tau) w^*_{,\alpha}(\mathbf{x}) d\Omega - \int\limits_{\Omega_s^i} I_Q \ddot{w}_3(\mathbf{x},\tau) w^*(\mathbf{x}) d\Omega +$$

$$+ \int\limits_{\Omega_s^i} q(\mathbf{x},\tau) w^*(\mathbf{x}) d\Omega = 0, \tag{14}$$

where $\partial\Omega_s^i$ is the boundary of the local subdomain and

$$M_\alpha(\mathbf{x},\tau) = M_{\alpha\beta}(\mathbf{x},\tau) n_\beta(\mathbf{x})$$

is the normal bending moment and n_α is the unit outward normal vector to the boundary $\partial\Omega_s^i$. The local weak-forms (13) and (14) are the starting point for deriving local boundary integral equations on the basis of appropriate test functions. Unit step functions are chosen for the test functions $w^*_{\alpha\beta}(\mathbf{x})$ and $w^*(\mathbf{x})$ in each subdomain

$$w^*_{\alpha\gamma}(\mathbf{x}) = \begin{cases} \delta_{\alpha\gamma} & \text{at } \mathbf{x} \in (\Omega_s \cup \partial\Omega_s) \\ 0 & \text{at } \mathbf{x} \notin (\Omega_s \cup \partial\Omega_s) \end{cases}, \quad w^*(\mathbf{x}) = \begin{cases} 1 & \text{at } \mathbf{x} \in (\Omega_s \cup \partial\Omega_s) \\ 0 & \text{at } \mathbf{x} \notin (\Omega_s \cup \partial\Omega_s) \end{cases}. \tag{15}$$

Then, the local weak-forms (13) and (14) are transformed into the following local integral equations (LIEs)

$$\int\limits_{\partial\Omega_s^i} M_\alpha(\mathbf{x},\tau)d\Gamma - \int\limits_{\Omega_s^i} Q_\alpha(\mathbf{x},\tau)d\Omega - \int\limits_{\Omega_s^i} I_M \ddot{w}_\alpha(\mathbf{x},\tau)d\Omega = 0, \tag{16}$$

$$\int\limits_{\partial\Omega_s^i} Q_\alpha(\mathbf{x},\tau)n_\alpha(\mathbf{x})d\Gamma - \int\limits_{\Omega_s^i} I_Q \ddot{w}_3(\mathbf{x},\tau)d\Omega + \int\limits_{\Omega_s^i} q(\mathbf{x},\tau)d\Omega = 0. \tag{17}$$

In the above local integral equations, the trial functions $w_\alpha(\mathbf{x},\tau)$ related to rotations, and $w_3(\mathbf{x},\tau)$ related to transversal displacements, are chosen as the moving least-squares (MLS) approximations over a number of nodes randomly spread within the domain of influence.

3 Numerical solution

In general, a meshless method uses a local interpolation to represent the trial function with the values (or the fictitious values) of the unknown variable at some randomly located nodes. The moving least-squares (MLS) approximation [Lancaster and Salkauskas, 1981; Nayroles et al., 1992; Belytschko, 1996] used in the present analysis may be considered as one of such schemes. Let us consider a sub-domain Ω_x of the problem domain Ω in the neighbourhood of a point $\mathbf{x}$ for the definition of the MLS approximation of the trial function around $\mathbf{x}$ (Fig. 2). To approximate the distribution of the generalized displacements (rotations and deflection) in Ω_x over a number of randomly located nodes $\{\mathbf{x}^a\}$, $a = 1,2,...n$, the MLS approximant $w_i^h(\mathbf{x},\tau)$ of $w_i(\mathbf{x},\tau)$ is defined by

$$\mathbf{w}^h(\mathbf{x},\tau) = \mathbf{p}^T(\mathbf{x})\tilde{\mathbf{a}}(\mathbf{x},\tau), \quad \forall \mathbf{x} \in \Omega_x, \tag{18}$$

where $\mathbf{w}^h = \left[w_1^h, w_2^h, w_3^h\right]^T$, $\mathbf{p}^T(\mathbf{x}) = \left[p^1(\mathbf{x}), p^2(\mathbf{x}), ..., p^m(\mathbf{x})\right]$ is a complete monomial basis of order m, and $\tilde{\mathbf{a}}(\mathbf{x},\tau) = \left[\mathbf{a}^1(\mathbf{x},\tau),\ \mathbf{a}^2(\mathbf{x},\tau),\ ...,\ \mathbf{a}^m(\mathbf{x},\tau)\right]^T$ is composed of vectors $\mathbf{a}^j(\mathbf{x},\tau) = \left[a_1^j(\mathbf{x},\tau),\ a_2^j(\mathbf{x},\tau),\ a_3^j(\mathbf{x},\tau)\right]^T$ which are functions of the spatial co-ordinates $\mathbf{x} = [x_1, x_2]^T$ and the time τ.

The coefficient vector $\tilde{\mathbf{a}}(\mathbf{x},\tau)$ is determined by minimizing a weighted discrete L_2-norm defined as

$$J(\mathbf{x}) = \sum_{a=1}^{n} v^a(\mathbf{x}) \left[\mathbf{p}^T(\mathbf{x}^a)\tilde{\mathbf{a}}(\mathbf{x},\tau) - \hat{\mathbf{w}}^a(\tau)\right]^2, \tag{19}$$

where $v^a(\mathbf{x}) > 0$ is the weight function associated with the node a and the square power is considered in the sense of scalar product. Recall that n is the number of nodes in Ω_x for which the weight function $v^a(\mathbf{x}) > 0$ and $\hat{\mathbf{w}}^a(\tau)$ are the fictitious nodal values, but not the nodal values of the unknown trial function $\mathbf{w}^h(\mathbf{x},\tau)$, in general. The stationarity of J in eq. (19) with respect to $\tilde{\mathbf{a}}(\mathbf{x},\tau)$ leads to

$$\mathbf{A}(\mathbf{x})\tilde{\mathbf{a}}(\mathbf{x},\tau) - \mathbf{B}(\mathbf{x})\hat{\mathbf{w}}(\tau) = 0\,, \tag{20}$$

where

$$\hat{\mathbf{w}}(\tau) = \left[\hat{\mathbf{w}}^1(\tau),\, \hat{\mathbf{w}}^2(\tau),\, ...,\, \hat{\mathbf{w}}^n(\tau)\right]^T,$$

$$\mathbf{A}(\mathbf{x}) = \sum_{a=1}^{n} v^a(\mathbf{x})\mathbf{p}(\mathbf{x}^a)\mathbf{p}^T(\mathbf{x}^a)\,,$$

$$\mathbf{B}(\mathbf{x}) = \left[v^1(\mathbf{x})\mathbf{p}(\mathbf{x}^1),\, v^2(\mathbf{x})\mathbf{p}(\mathbf{x}^2), ..., v^n(\mathbf{x})\mathbf{p}(\mathbf{x}^n)\right]\,. \tag{21}$$

The solution of eq. (20) for $\tilde{\mathbf{a}}(\mathbf{x},\tau)$ and the subsequent substitution into eq. (18) lead to the following expression

$$\mathbf{w}^h(\mathbf{x},\tau) = \mathbf{\Phi}^T(\mathbf{x})\cdot\hat{\mathbf{w}}(\tau) = \sum_{a=1}^{n}\phi^a(\mathbf{x})\hat{\mathbf{w}}^a(\tau)\,, \tag{22}$$

where

$$\mathbf{\Phi}^T(\mathbf{x}) = \mathbf{p}^T(\mathbf{x})\mathbf{A}^{-1}(\mathbf{x})\mathbf{B}(\mathbf{x})\,. \tag{23}$$

In eq. (22), $\phi^a(\mathbf{x})$ is usually referred to as the shape function of the MLS approximation corresponding to the nodal point $\mathbf{x}^a$. From eqs. (21) and (23), it can be seen that $\phi^a(\mathbf{x}) = 0$ when $v^a(\mathbf{x}) = 0$. In practical applications, $v^a(\mathbf{x})$ is often chosen in such a way that it is non-zero over the support of the nodal point $\mathbf{x}_i$. The support of the nodal point $\mathbf{x}^a$ is usually taken to be a circle of the radius r_i centred at $\mathbf{x}^a$ (see Fig. 2). The radius r_i is an important parameter of the MLS approximation because it determines the range of the interaction (coupling) between the degrees of freedom defined at considered nodes.

A 4^{th}-order spline-type weight function is applied in the present work

$$v^a(\mathbf{x}) = \begin{cases} 1 - 6\left(\frac{d^a}{r^a}\right)^2 + 8\left(\frac{d^a}{r^a}\right)^3 - 3\left(\frac{d^a}{r^a}\right)^4 & 0 \le d^a \le r^a \\ 0 & d^a \ge r^a \end{cases}, \tag{24}$$

where $d^a = \|\mathbf{x} - \mathbf{x}^a\|$ and r^a is the radius of the circular support domain. With eq. (24), the C^1-continuity of the weight function is ensured over the entire domain, therefore the continuity condition of the bending moments and the shear forces is satisfied. The size of the support r^a should be large enough to cover a sufficient number of nodes in the domain of definition to ensure the regularity of the matrix $\mathbf{A}$. The value of n is determined by the number of nodes lying in the support domain with radius r^a.

The partial derivatives of the MLS shape functions are obtained as [Atluri, 2004]

$$\phi^a_{,k} = \sum_{j=1}^{m} \left[p^j_{,k} (\mathbf{A}^{-1}\mathbf{B})^{ja} + p^j (\mathbf{A}^{-1}\mathbf{B}_{,k} + \mathbf{A}^{-1}_{,k}\mathbf{B})^{ja} \right], \tag{25}$$

wherein $\mathbf{A}^{-1}_{,k} = \left(\mathbf{A}^{-1}\right)_{,k}$ represents the derivative of the inverse of $\mathbf{A}$ with respect to x_k, which is given by

$$\mathbf{A}^{-1}_{,k} = -\mathbf{A}^{-1}\mathbf{A}_{,k}\mathbf{A}^{-1}.$$

The directional derivatives of $\mathbf{w}(\mathbf{x},\tau)$ are approximated in terms of the same nodal values as

$$\mathbf{w}_{,k}(\mathbf{x},\tau) = \sum_{a=1}^{n} \hat{\mathbf{w}}^a(\tau)\phi^a_{,k}(\mathbf{x}). \tag{26}$$

Substituting the approximation (26) into the definition of the bending moments (6) and then using $M_\alpha(\mathbf{x},\tau) = M_{\alpha\beta}(\mathbf{x},\tau)n_\beta(\mathbf{x})$, one obtains for

$$\mathbf{M}(\mathbf{x},\tau) = \left[M_1(\mathbf{x},\tau), \quad M_2(\mathbf{x},\tau)\right]^T$$

$$\mathbf{M}(\mathbf{x},\tau) = \mathbf{N_1}\sum_{a=1}^{n}\mathbf{B}^a_1(\mathbf{x})\mathbf{w}^{*a}(\tau) + \mathbf{N_2}\sum_{a=1}^{n}\mathbf{B}^a_2(\mathbf{x})\mathbf{w}^{*a}(\tau) = \mathbf{N}_\alpha(\mathbf{x})\sum_{a=1}^{n}\mathbf{B}^a_\alpha(\mathbf{x})\mathbf{w}^{*a}(\tau), \tag{27}$$

where the vector $\mathbf{w}^{*a}(\tau)$ is defined as a column vector $\mathbf{w}^{*a}(\tau) = [\hat{w}^a_1(\tau), \, \hat{w}^a_2(\tau)]^T$, the matrices $\mathbf{N}_\alpha(\mathbf{x})$ are related to the normal vector $\mathbf{n(x)}$ on $\partial\Omega_s$ by

$$\mathbf{N}_1(\mathbf{x}) = \begin{bmatrix} n_1 & 0 & n_2 \\ 0 & n_2 & n_1 \end{bmatrix}$$

and

$$\mathbf{N}_2(\mathbf{x}) = \begin{bmatrix} C_{11} & 0 \\ 0 & C_{22} \end{bmatrix} \begin{bmatrix} n_1 & n_1 \\ n_2 & n_2 \end{bmatrix},$$

and the matrices $\mathbf{B}^a_\alpha$ are represented by the gradients of the shape functions as

$$\mathbf{B}^a_1(\mathbf{x}) = \begin{bmatrix} 2D_{11}\phi^a_{,1} & 0 \\ 0 & 2D_{22}\phi^a_{,2} \\ D_{12}\phi^a_{,2} & D_{12}\phi^a_{,1} \end{bmatrix}, \quad \mathbf{B}^a_2(\mathbf{x}) = \begin{bmatrix} \phi^a_{,1} & 0 \\ 0 & \phi^a_{,2} \end{bmatrix}.$$

The influence of the material properties for composite laminates is incorporated into $C_{\alpha\beta}$ and $D_{\alpha\beta}$ defined in equations (7).
Similarly one can obtain the approximation for the shear forces

$$\mathbf{Q}(\mathbf{x},\tau) = \mathbf{C}(\mathbf{x}) \sum_{a=1}^{n} [\phi^a(\mathbf{x})\mathbf{w}^{*a}(\tau) + \mathbf{F}^a(\mathbf{x})\hat{w}_3^a(\tau)], \tag{28}$$

where $\mathbf{Q}(\mathbf{x},\tau) = [Q_1(\mathbf{x},\tau),\, Q_2(\mathbf{x},\tau)]^T$ and

$$\mathbf{C}(\mathbf{x}) = \begin{bmatrix} C_1(\mathbf{x}) & 0 \\ 0 & C_2(\mathbf{x}) \end{bmatrix}, \quad \mathbf{F}^a(\mathbf{x}) = \begin{bmatrix} \phi^a_{,1} \\ \phi^a_{,2} \end{bmatrix}.$$

Then, insertion of the MLS-discretized moment and force fields (27) and (28) into the local integral equations (16) and (17) yields the discretized local integral equations

$$\sum_{a=1}^{n} \left[\int_{L_s^i + \Gamma_{sw}^i} \mathbf{N}_\alpha(\mathbf{x})\mathbf{B}_\alpha^a(\mathbf{x}) d\Gamma - \int_{\Omega_s^i} \mathbf{C}(\mathbf{x})\phi^a(\mathbf{x}) d\Omega \right] \mathbf{w}^{*a}(\tau) -$$

$$- \sum_{a=1}^{n} I_M \ddot{\mathbf{w}}^{*a}(\tau) \left(\int_{\Omega_s^i} \phi^a(\mathbf{x}) d\Omega \right) -$$

$$- \sum_{a=1}^{n} \hat{w}_3^a(\tau) \left(\int_{\Omega_s^i} \mathbf{C}(\mathbf{x})\mathbf{F}^a(\mathbf{x}) d\Omega \right) = - \int_{\Gamma_{sM}^i} \tilde{\mathbf{M}}(\mathbf{x},\tau) d\Gamma, \tag{29}$$

$$\sum_{a=1}^{n} \left(\int_{\partial\Omega_s^i} \mathbf{C}_n(\mathbf{x})\phi^a(\mathbf{x}) d\Gamma \right) \mathbf{w}^{*a}(\tau) + \sum_{a=1}^{n} \hat{w}_3^a(\tau) \left(\int_{\partial\Omega_s^i} \mathbf{C}_n(\mathbf{x})\mathbf{F}^a(\mathbf{x}) d\Gamma \right) =$$

$$-I_Q \sum_{a=1}^{n} \ddot{\hat{w}}_3^a(\tau) \left(\int_{\Omega_s^i} \phi^a(\mathbf{x}) d\Omega \right) = - \int_{\Omega_s^i} q(\mathbf{x},\tau) d\Omega, \tag{30}$$

in which $\tilde{\mathbf{M}}(\mathbf{x},\tau)$ represent the prescribed bending moments on Γ_{sM}^i and

$$\mathbf{C}_n(\mathbf{x}) = (n_1,\, n_2) \begin{pmatrix} C_1 & 0 \\ 0 & C_2 \end{pmatrix} = (C_1 n_1,\, C_2 n_2).$$

Equations (29) and (30) are considered on the subdomains adjacent to the interior nodes $\mathbf{x}^i$ as well as to the boundary nodes on Γ^i_{sM}.

For the source point $\mathbf{x}^i$ located on the global boundary Γ the boundary of the subdomain $\partial\Omega^i_s$ is decomposed into L^i_s and Γ^i_{sM} (part of the global boundary with prescribed bending moment) according to Fig. 2.

It should be noted here that there are neither Lagrange multipliers nor penalty parameters introduced into the local weak-forms (11) and (12) because the essential boundary conditions on Γ^i_{sw} (part of the global boundary with prescribed rotations or displacements) can be imposed directly, using the interpolation approximation (22)

$$\sum_{a=1}^{n} \phi^a(\mathbf{x}^i)\hat{\mathbf{w}}^a(\tau) = \tilde{\mathbf{w}}(\mathbf{x}^i,\tau) \tag{31}$$

for $\mathbf{x}^i \in \Gamma^i_{sw}$, where $\tilde{w}(\mathbf{x}^i,\tau)$ is the generalized displacement vector prescribed on the boundary Γ^i_{sw}. For a clamped plate all three vector components (rotations and deflection) are vanishing on the fixed edge, and eq. (31) is used at all the boundary nodes in such a case. However, for a simply supported plate only the third component of the displacement vector (deflection) is prescribed, while the rotations are unknown. Then, the entire equation (29) and the third component of eq. (31) are applied to the nodes lying on the global boundary. On those parts of the global boundary where no displacement boundary conditions are prescribed both local integral equations (29) and (30) are applied.

Collecting the discretized local boundary-domain integral equations together with the discretized boundary conditions for the generalized displacements, one obtains a complete system of ordinary differential equations and it can be rearranged in such a way that all known quantities are on the r.h.s. Thus, in matrix form the system becomes

$$\mathbf{A}\ddot{\mathbf{x}} + \mathbf{C}\mathbf{x} = \mathbf{Y}. \tag{32}$$

Recall that the system matrix has a block structure. There are many time integration procedures for the solution of this system of ordinary differential equations. In the present work, the Houbolt method is applied. In the Houbolt finite-difference scheme [Houbolt (1950)], the "acceleration" $\ddot{\mathbf{x}}$ is expressed as

$$\ddot{\mathbf{x}}_{\tau+\Delta\tau} = \frac{2\mathbf{x}_{\tau+\Delta\tau} - 5\mathbf{x}_{\tau} + 4\mathbf{x}_{\tau-\Delta\tau} - \mathbf{x}_{\tau-2\Delta\tau}}{\Delta\tau^2}, \tag{33}$$

where $\Delta\tau$ is the time-step.

Substituting eq. (33) into eq. (32), we obtain the following system of algebraic equations for the unknowns $\mathbf{x}_{\tau+\Delta\tau}$

$$\left[\frac{2}{\Delta\tau^2}\mathbf{A}+\mathbf{C}\right]\mathbf{x}_{\tau+\Delta\tau}=\frac{1}{\Delta\tau^2}5\mathbf{A}\mathbf{x}_\tau+\mathbf{A}\frac{1}{\Delta\tau^2}\left\{-4\mathbf{x}_{\tau-\Delta\tau}+\mathbf{x}_{\tau-2\Delta\tau}\right\}+\mathbf{Y}. \tag{34}$$

The value of the time-step has to be appropriately selected with respect to material parameters (elastic wave velocities) and time dependence of the boundary conditions.

4 Numerical examples

In this section, numerical results are presented for laminate plates under a mechanical load. In order to test the accuracy, the numerical results obtained by the present method are compared with the results provided by the FEM-ANSYS code using a very fine mesh. Clamped and simply supported square plates are analysed. In all numerical calculations, deviations of the results for plates with a laminate structure from those corresponding to a homogeneous plate are investigated. The mass density is assumed to be uniform within the whole bulk of the plate.

4.1 Clamped square plate

Consider a clamped square plate with a side-length $a=0.254m$ and the plate thicknesses $h/a=0.05$. The plate is subjected to a uniformly distributed static load. Homogeneous material properties are considered firstly to test the accuracy of the present computational method. The following material parameters are used in our numerical analysis: Young's moduli $E_2=0.6895\cdot10^{10}\,\mathrm{N/m^2}$ and $E_1=2E_2$, Poisson's ratios $\nu_{21}=0.15$ and $\nu_{12}=0.3$ and mass density $\rho=5.0\times10^3\,\mathrm{kgm^{-3}}$. The used shear moduli correspond to Young's modulus E_2, namely, $G_{12}=G_{13}=G_{23}=E_2/\left[2(1+\nu_{12})\right]$.

In our numerical calculations, 441 nodes with a regular distribution were used for the approximation of the rotations and the deflection. The origin of the coordinate system is located at the center of the plate. The variation of the deflection with the x_1-coordinate at $x_2=0$ of the plate is presented in Fig. 3. The deflection value is normalized by the corresponding central deflection of an isotropic plate with material constants given above but $E_1=E_2$. For a uniformly distributed load $q_0=300\,\mathrm{psi}=2.07\times10^6\,\mathrm{Nm^{-2}}$ we have $w_3^{iso}(0)=8.842\cdot10^{-3}m$. The numerical results are compared with the results obtained by the FEM-ANSYS code with a very fine mesh of 900 quadrilateral eight-node shell elements for a quarter of the plate. Our numerical results are in a very good agreement with those obtained by the FEM for an orthotropic plate. One can observe that the deflection value is reduced for an orthotropic plate if one of the Young's moduli is increased. This is due to the increase of the plate stiffness for the orthotropic plate.

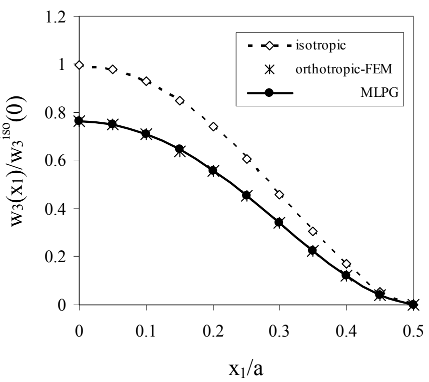

Figure 3: Variation of the deflection with the x_1-coordinate for a clamped homogeneous square plate

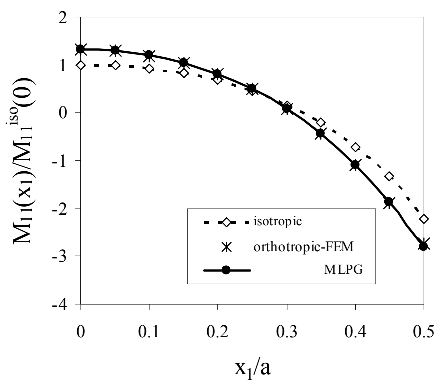

Figure 4: Variation of the bending moment with the x_1-coordinate for a clamped homogeneous square plate

The variation of the bending moment M_{11} is presented in Fig. 4. Here, the bending moment is normalized by the central bending moment value corresponding to an isotropic plate $M_{11}^{iso}(0) = 3064Nm$. The absolute values of the bending moment at the plate center (0,0) and the center of the clamped side (0.5a,0) are higher than in the isotropic case.

Next, a clamped orthotropic thick square plate under an impact load with Heaviside time variation is analyzed. The used geometrical and material parameters are the same as in the static case. For the numerical modelling we have used again 441 nodes with a regular distribution. Numerical calculations are carried out for a time-step $\Delta\tau = 0.357 \cdot 10^{-4}s$. The MLPG results are compared with those obtained by FEM-ANSYS computer code, where 900 quadrilateral eight-node shell elements with 1000 time increments have been used. The time variations of the central deflection and the bending moment M_{11} are given in Fig. 5 and Fig. 6, respectively. Both quantities are normalized by their corresponding static values at the center of the isotropic plate. The static central deflection is $w_3^{stat}(0) = 8.842 \cdot 10^{-3}m$ for the considered load $q_0 = 2.07 \times 10^6\,\mathrm{Nm}^{-2}$. The static bending moment is $M_{11}^{stat}(0) = 3064Nm$. The time is normalized by $\tau_0 = a^2/4\sqrt{\rho h/D} = 0.3574 \cdot 10^{-2}s$. A good agreement of the present results for the deflection and the bending moment at the plate center and the FEM results is observed in both figures.

The peaks of the moment amplitudes are shifted to shorter time instants for the or-

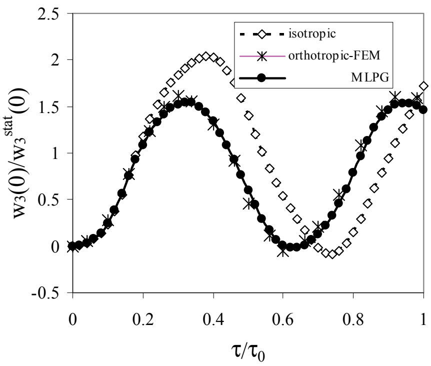

Figure 5: Time variation of the deflection at the center of a clamped square plate subjected to a suddenly applied load

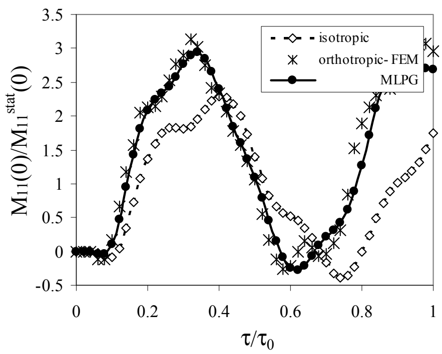

Figure 6: Time variation of the bending moment at the center of a clamped square plate subjected to a suddenly applied load

thotropic plate with a larger flexural rigidity. Since the mass density is the same for both isotropic and orthotropic plates, the wave velocity is higher for the orthotropic plate with higher Young's modulus. The amplification of the bending moments due to the dynamic impact load for both isotropic and orthotropic plates are almost the same if they are normalized with respect to the corresponding static values. The static bending moment for the orthotropic plate is slightly higher at the center of the plate (see Fig. 4). Then, the peak value for the orthotropic plate under an impact load in Fig. 6 has to be higher since that value is normalized by the isotropic bending moment.

Next, a clamped three-ply square plate under a uniform static load is analyzed. The used geometrical parameters are the same as in the previous homogeneous case. The total plate thickness is $h = 0.0127m$, which is equal to the thickness of the homogeneous plate in previous examples. The bottom and top layers have the same thickness $h_1 = h_3 = h/4$. Young's moduli for both bottom and top layers are the same and they are 5 times larger than that ones corresponding to the homogeneous orthotropic plate. The second mid-layer has the thickness $h_2 = h/2$ and the same material properties as the homogeneous plate analyzed in previous examples. For the numerical modelling we have used again 441 nodes with a regular distribution. The variation of the deflection with the x_1-coordinate at $x_2 = 0$ of the plate is presented in Fig. 7. The deflection value is normalized by the corresponding central deflection of an isotropic homogeneous plate. The numerical results for the laminated orthotropic plate are compared with the results obtained by the FEM-

ANSYS code with a very fine mesh of 900 quadrilateral eight-node shell elements for a quarter of the plate. Our numerical results are in a very good agreement with those obtained by the FEM. One can observe that the deflection value is reduced for the laminated orthotropic plate due to the larger flexural rigidity.

The variation of the bending moment M_{11} is presented in Fig. 8. Here, the bending moment is normalized by the central bending moment value corresponding to an isotropic homogeneous plate $M_{11}^{iso}(0) = 3064Nm$. By comparing the bending moments for the orthotropic homogeneous plate shown in Fig. 4 with results for orthotropic laminate plate presented in Fig. 8, it can be concluded that the results are very similar. It means that the considered lamination has a vanishing influence on the bending moment variation.

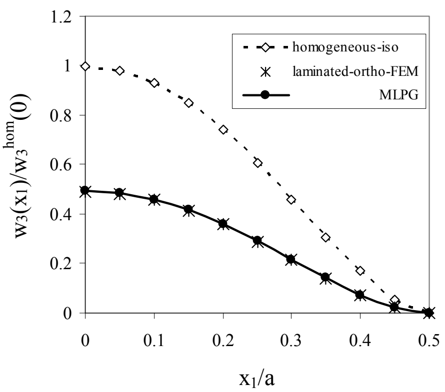

Figure 7: Variation of the deflection with the x_1-coordinate for a clamped laminated square plate

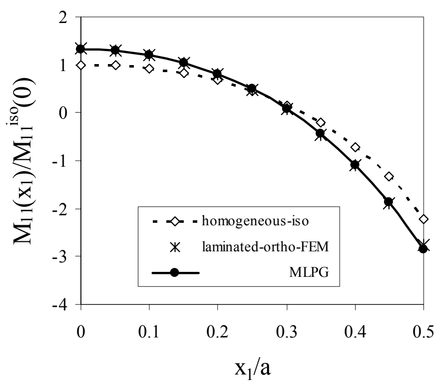

Figure 8: Variation of the bending moment with the x_1-coordinate for a clamped laminated square plate

Next, a clamped orthotropic laminated square plate under an impact load with Heaviside time variation is analyzed. The used geometrical and material parameters are the same as in the previous static case. Numerical calculations are carried out for a time-step $\Delta\tau = 0.357 \cdot 10^{-4} s$. The MLPG results are compared with those obtained by FEM-ANSYS computer code. The time variations of the central deflection and the bending moment M_{11} are given in Fig. 9 and Fig. 10, respectively. Both quantities are normalized by their corresponding static values at the center of the isotropic homogeneous plate. The time is normalized by $\tau_0 = 0.3574 \cdot 10^{-2} s$. A good agreement of the present results for the deflection and the bending moment at the plate center and the FEM results is observed in both figures.

The peaks of the deflection amplitudes are shifted to shorter time instants for the

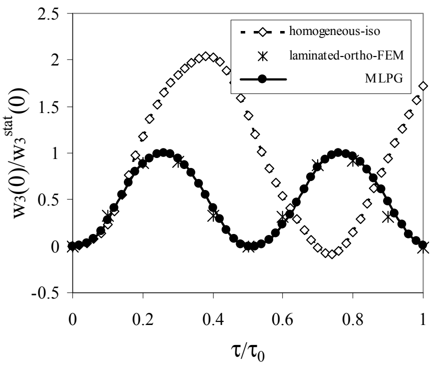

Figure 9: Time variation of the deflection at the center of a clamped laminated plate subjected to a suddenly applied load

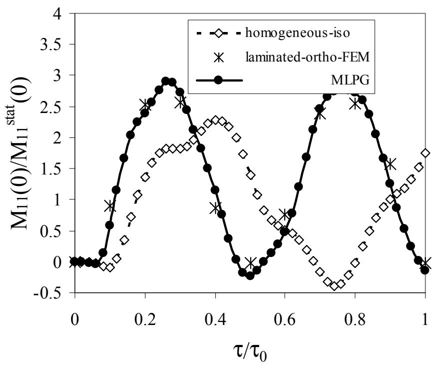

Figure 10: Time variation of the bending moment at the center of a clamped laminated plate subjected to a suddenly applied load

laminated orthotropic plate with a larger flexural rigidity. Since the mass density is the same for both isotropic homogeneous and orthotropic laminated plates, the wave velocity is higher for the laminated orthotropic plate with higher Young‘s moduli. The peaks values are reduced for the laminated orthotropic plate since the corresponding static values are also reduced with respect to the corresponding isotropic homogeneous plate. However, an amplification of the bending moment for the laminated orthotropic plate is observed. The reason for the shifting peak values of the bending moment to shorter time instants is the same as that for the deflection peaks.

4.2 Simply supported three-ply orthotropic square plate

A simply supported three-ply orthotropic square plate under a uniform static load is then analyzed. The used geometrical and material parameters are the same as for the previous clamped plate. For the numerical modelling we have used again 441 nodes with a regular distribution. A uniformly distributed load $q_0 = 300\,psi = 2.07 \times 10^6\,\mathrm{Nm}^{-2}$ is considered here. The deflection value is normalized by the corresponding central deflection of an isotropic homogeneous plate $w_3^{iso}(0) = 0.02829m$. The variation of the deflection with the x_1-coordinate at $x_2 = 0$ of the plate is presented in Fig. 11. One can observe that the deflection value is reduced for the homogeneous orthotropic plate due to the larger flexural rigidity. A higher deflection reduction is obtained for laminated orthotropic plate due to a further increase of the flexural rigidity.

The variation of the bending moment M_{11} is shown in Fig. 12. The bending moment at the center of the plate $M_{11}^{iso}(0) = 6482Nm$ is used as a normalization parameter. The bending moment is enlarged for the orthotropic homogeneous or laminated plates with respect to the moment for an isotropic homogeneous plate. Here again, the lamination has a vanishing influence on the bending moment.

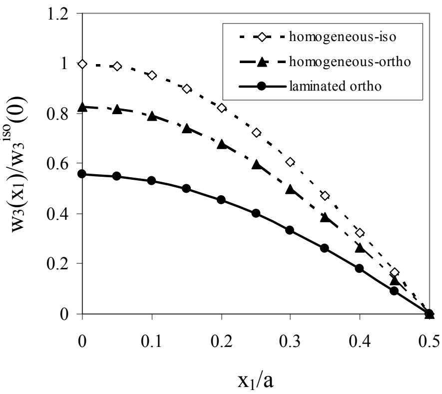

Figure 11: Variation of the deflection with the x_1-coordinate for simply supported square plates

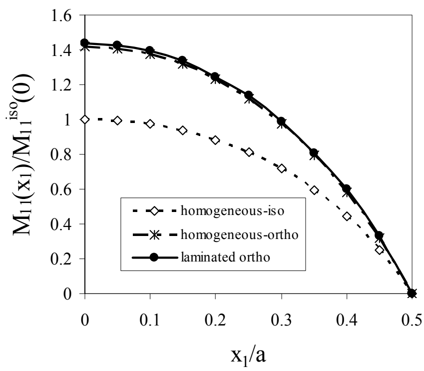

Figure 12: Variation of the bending moment with the x_1-coordinate for simply supported square plates

Finally, a simply supported three-ply laminated orthotropic square plate under an impact load with Heaviside time variation is analyzed. The used geometrical and material parameters are the same as in the previous static case. In the numerical modelling, again 441 nodes with a regular distribution have been used. Numerical calculations are carried out for a time-step $\Delta\tau = 0.357 \cdot 10^{-4}s$. The time variations of the central deflection and the bending moment M_{11} are given in Fig. 13 and Fig. 14, respectively. Both quantities are normalized by their corresponding static values at the center of the isotropic homogeneous plate. The static central deflection is $w_3^{stat}(0) = 0.02829m$ for the considered load $q_0 = 2.07 \times 10^6\,\mathrm{Nm}^{-2}$. The static bending moment is$M_{11}^{stat}(0) = 6482Nm$. The time is normalized by $\tau_0 = 0.3574 \cdot 10^{-2}s$.

The peaks of the deflection and bending moment amplitudes are shifted to shorter time instants for the orthotropic homogeneous and laminated plates due to larger Young‘s moduli. They are largest for the laminated orthotropic plate. Since the mass density is the same in all plates, the elastic wave velocity is largest for the laminated plate. The maximum reduction of the deflection is achieved for the laminate plate, where the flexural rigidity is the largest. Here, one can observe again that the lamination has practically no influence on the bending moment. Therefore,

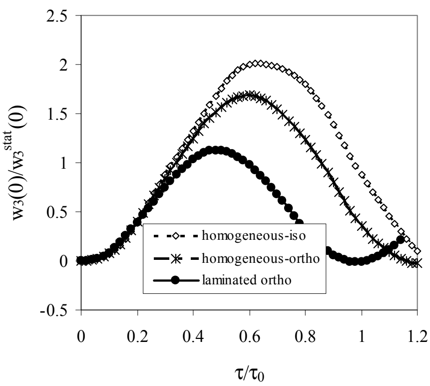

Figure 13: Time variation of the deflection at the center of a simply supported plates subjected to a suddenly applied load

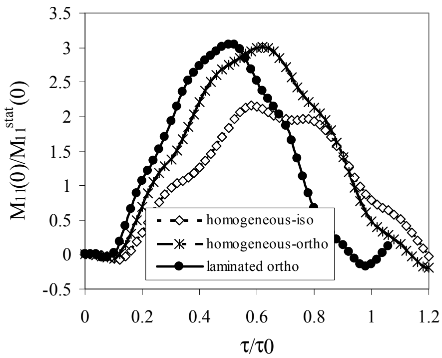

Figure 14: Time variation of the bending moment at the center of simply supported plates subjected to a suddenly applied load

the peak values for the bending moment in laminated and homogeneous plates have almost the same value (Fig. 14).

5 Conclusions

A meshless local Petrov-Galerkin method is applied to laminate plates under mechanical loadings. Both stationary and impact loads are considered. The present computational method has no restriction on the number of the laminae and their material properties. The laminate plate bending problem is described by the Reissner-Mindlin theory. The Reissner-Mindlin theory reduces the original three-dimensional (3-D) thick plate problem to a 2-D problem. Nodal points are randomly distributed over the mean surface of the considered plate. Each node is the center of a circle surrounding this node. The weak-form on small subdomains with a Heaviside step function as the test functions is applied to derive local integral equations. After performing the spatial MLS approximation, a system of ordinary differential equations for certain nodal unknowns is obtained. Then, the system of the ordinary differential equations of the second order resulting from the equations of motion is solved by the Houbolt finite-difference scheme as a time-stepping method.

The proposed method is a truly meshless method, which requires neither domain elements nor background cells in either the interpolation or the integration. It is demonstrated numerically that the quality of the results obtained by the proposed MLPG method is very good. The degree of the agreement of our numerical results with those obtained by the FEM-ANSYS computer code ranges from good to excellent. Since in our illustrative examples only simple problems are analysed, only a regular node distribution has been used. However, a random location of nodes should be considered for general boundary value problems. To this end, an efficient random node generator is required, which has to be developed for further progress of the method.

Acknowledgement: The authors gratefully acknowledge the support by the Slovak Science and Technology Assistance Agency registered under number APVV-0427-07, the Slovak Grant Agency VEGA-2/0039/09, and the German Research Foundation (DFG, Project-No ZH 15/11-1).

References

Atluri, S.N.; Zhu, T. (1998): A new Meshless Local Petrov-Galerkin (MLPG) approach in computational mechanics. *Computational Mechanics*, 22: 117-127.

Atluri, S.N.; Sladek, J.; Sladek, V.; Zhu, T. (2000): The local boundary integral equation (LBIE) and its meshless implementation for linear elasticity. *Computational Mechanics*, 25: 180-198.

Atluri, S. N. (2004): *The Meshless Method, (MLPG) For Domain & BIE Discretizations*, Tech Science Press.

Atluri, S.N.; Han, Z.D.; Shen, S. (2003): Meshless local Petrov-Galerkin (MLPG) approaches for solving the weakly-singular traction & displacement boundary integral equations. *CMES: Computer Modeling in Engineering & Sciences*, 4: 507-516.

Atluri, S.N.; Shen, S. (2005): Simulation of a 4^{th} order ODE: Illustartion of various primal & mixed MLPG methods. *CMES: Computer Modeling in Engineering & Sciences*, 7 (3): 241-268.

Atluri, S.N.; Liu, H.T.; Han, Z.D. (2006a): Meshless local Petrov-Galerkin (MLPG) mixed collocation method for elasticity problems. *CMES: Computer Modeling in Engineering & Sciences*, 14 (3): 141-152.

Atluri, S.N.; Liu, H.T.; Han, Z.D. (2006b): Meshless local Petrov-Galerkin (MLPG) mixed finite difference method for solid mechanics. *CMES: Computer Modeling in Engineering & Sciences*, 15 (1): 1-16.

Belytschko, T.; Krogauz, Y.; Organ, D.; Fleming, M.; Krysl, P. (1996): Meshless methods; an overview and recent developments. *Comp. Meth. Appl. Mech. Engn.*, 139: 3-47.

Ching, H.K.; Chen, J.K. (2006): Thermomechanical analysis of functionally graded composites under laser heating by the MLPG method. *CMES: Computer*

Modeling in Engineering & Sciences, 13 (3): 199-217.

De Leon, S.; Paris, F. (1987): Analysis of thermal stresses in plates with boundary element method. *Engineering Analysis with Boundary Elements*, 4: 199-203.

Gao, L.; Liu, K.; Liu, Y. (2006): Applications of MLPG method in dynamic fracture problems. *CMES: Computer Modeling in Engineering & Sciences*, 12 (3): 181-195.

Han, Z.D.; Atluri, S.N. (2004a): Meshless local Petrov-Galerkin (MLPG) approaches for solving 3D problems in elasto-statics. *CMES: Computer Modeling in Engineering & Sciences*, 6: 169-188.

Han, Z.D.; Atluri, S.N. (2004b): A meshless local Petrov-Galerkin (MLPG) approach for 3-dimensional elasto-dynamics. *CMC: Computers, Materials & Continua*, 1: 129-140.

Han, Z.D.; Rajendran, A.M.; Atluri, S.N. (2005): Meshless Local Petrov-Galerkin (MLPG) approaches for solving nonlinear problems with large deformations and rotations. *CMES: Computer Modeling in Engineering & Sciences*, 10 (1): 1-12.

Han, Z.D.; Liu, H.T.; Rajendran, A.M.; Atluri, S.N. (2006): The applications of Meshless Local Petrov-Galerkin (MLPG) approaches in high-speed impact, penetration and perforation problems. *CMES: Computer Modeling in Engineering & Sciences*, 14 (2): 119-128.

Houbolt, J.C. (1950): A recurrence matrix solution for the dynamic response of elastic aircraft. *Journal of Aeronautical Sciences*, 17: 371-376.

Jarak, T.; Soric, J.; Hoster, J. (2007): Analysis of shell deformation responses by the Meshless Local Petrov-Galerkin (MLPG) approach. *CMES: Computer Modeling in Engineering & Sciences*, 18 (3): 235-246.

Lancaster, P.; Salkauskas, T. (1981): Surfaces generated by moving least square methods. *Math. Comput.*, 37: 141-158.

Lekhnitskii, S.G. (1963): *Theory of Elasticity of an Anisotropic Body.* Holden Day.

Liu, H.T.; Han, Z.D.; Rajendran, A.M.; Atluri, S.N. (2006): Computational modelling of impact response with the RG damage model and the meshless local Petrov-Galerkin (MLPG) approaches. *CMC: Computers, Materials & Continua*, 4: 43-53.

Long, S.Y.; Atluri, S.N. (2002): A meshless local Petrov Galerkin method for solving the bending problem of a thin plate. *CMES: Computer Modeling in Engineering & Sciences*, 3: 11-51.

Mau, S.T.; Tong, P.; Pian, T.H.H. (1972): Finite element solutions for laminated plates. *Journal of Composite Materials*, 6: 304-311.

Mikhailov, S.E. (2002): Localized boundary-domain integral formulations for problems with variable coefficients. *Eng. Analysis with Boundary Elements*, 26: 681-690.

Mindlin, R.D. (1951): Influence of rotary inertia and shear on flexural motions of isotropic, elastic plates. *Journal of Applied Mechanics ASME*, 18: 31-38.

Murakami, H. (1986): Laminated composite plate theory with improved in-plane responses. *Journal of Applied Mechanics ASME*, 53: 661-666.

Nayroles, B.; Touzot, G.; Villon, P. (1992): Generalizing the finite element method. *Computational Mechanics*, 10: 307-318.

Nie, Y.F.; Atluri, S.N.; You, C.W. (2006): The optimal radius of the support of radial weights used in Moving Least Squares approximation. *CMES: Computer Modeling in Engineering & Sciences*, 12 (2): 137-147.

Pagano, N.J. (1969): Exact solutions for composite laminates in cylindrical bending. *Journal of Composite Materials*, 3: 398-411.

Providakis, C.P. (2007): The effect of internal support conditions to the elesto-plastic transient response of Reissner-Mindlin plates. *CMES: Computer Modeling in Engineering & Sciences*, 18 (3): 247-258.

Qian, L.F.; Batra, R.C.; Chen, L.M. (2004): Analysis of cylindrical bending thermoelastic deformations of fuctionally graded plates by a meshless local Petrov-Galerkin method. *Computational Mechanics*, 33: 263-273.

Reddy J.N. (1997): *Mechanics of Laminated Composite Plates: Theory and Analysis*. CRC Press, Boca Raton.

Reissner, E. (1946): Stresses and small displacements analysis of shallow shells-II. *Journal Math. Physics*, 25: 279-300.

Sellountos, E.J.; Vavourakis, V.; Polyzos, D. (2005): A new singular/hypersingular MLPG (LBIE) method for 2D elastostatics. *CMES: Computer Modeling in Engineering & Sciences*, 7: 35-48.

Sladek, J.; Sladek, V.; Mang, H.A. (2002): Meshless formulations for simply supported and clamped plate problems. *Int. J. Num. Meth. Engn.*, 55: 359-375.

Sladek, J.; Sladek, V.; Mang, H.A. (2003): Meshless LBIE formulations for simply supported and clamped plates under dynamic load. *Computers and Structures*, 81: 1643-1651.

Sladek, J.; Sladek, V.; Wen, P.; Aliabadi, M.H. (2006): Meshless Local Petrov-Galerkin (MLPG) Method for shear deformable shells analysis. *CMES: Computer Modeling in Engineering & Sciences*, 13, 2006, 103-118.

Sladek, J.; Sladek, V.; Krivacek, J.; Wen, P.; Zhang, Ch. (2007): Meshless

Local Petrov-Galerkin (MLPG) method for Reissner-Mindlin plates under dynamic load. *Computer Meth. Appl. Mech. Engn.*, 196: 2681-2691.

Smojver, I.; Soric, J. (2007): Numerical modelling of damage response of layered composite plates. *CMC: Computers, Materials & Continua*, 5: 13-24.

Soric, J.; Li, Q.; Atluri, S.N. (2004): Meshless local Petrov-Galerkin (MLPG) formulation for analysis of thick plates. *CMES: Computer Modeling in Engineering & Sciences*, 6: 349-357.

Suetake, Y. (2006): Plate bending analysis by using a modified plate theory. *CMES: Computer Modeling in Engineering & Sciences,* 11 (3): 103-110.

Vavourakis, V.; Polyzos, D. (2007): A MLPG4 (LBIE) formulation in elastostatics. *CMC: Computers, Materials & Continua*, 5: 185-196.

Vel, S.; Batra, R.C. (1999): Analytical solution of rectangular thick plates subjected to arbitrary boundary conditions. *AIAA Journal*, 37: 1464-1473.

Vel, S.; Batra, R.C. (2000): The generalized plane strain deformations of thick anisotropic composite laminated plates. *International Journal of Solids and Structures*, 37: 715-733.

Vel, S.; Batra, R.C. (2001): Generalized plane strain thermoelastic deformation of laminated anisotropic thick plates. *International Journal of Solids and Structures*, 38: 1395-1414.

Wang J.; Huang M. (1991): Boundary element method for orthotropic thick plates. *Acta Mechanica Sinica*, 7: 258-266.

Wang J.; Schweizerhof K. (1996): Study on free vibration of moderately thick orthotropic laminated shallow shells by boundary-domain elements. *Applied Mathematical Modelling,* 20: 579-584.

Wen, P.H.; Hon, Y.C. (2007): Geometrically nonlinear analysis of Reissener-Mindlin plate by meshless computation. *CMES: Computer Modeling in Engineering & Sciences*, 21(3): 177-191.

Wu, X.H.; Shen, S.P.; Tao, W.Q. (2007): Meshless Local Petrov-Galerkin collocation method for two-dimensional heat conduction problems. *CMES: Computer Modeling in Engineering & Sciences*, 22 (1): 65-76.

Yuan, W.; Chen, P.; Liu, K. (2007): A new quasi-unsymmetric sparse linear systems solver for Meshless Local Petrov-Galerkin method (MLPG). *CMES: Computer Modeling in Engineering & Sciences*, 17 (2): 115-134.